

# Small-Angle Neutron Scattering of Solutions of Arborescent Graft Polystyrenes

Sangwook Choi and Robert M. Briber\*

Department of Materials and Nuclear Engineering, University of Maryland,  
College Park, Maryland 20742-2115

Barry J. Bauer and Andreas Topp

Polymers Division, National Institute of Standards and Technology,  
Gaithersburg, Maryland 20899-8542

Mario Gauthier and Lilian Tichagwa

Institute for Polymer Research, Department of Chemistry, University of Waterloo,  
Waterloo, Ontario N2L 3G1, Canada

Received February 10, 1999; Revised Manuscript Received July 29, 1999

**ABSTRACT:** Small-angle neutron scattering was used to measure the size and shape of arborescent graft polymers as a function of generation in solution. The radius of gyration of arborescent graft polymers was found to be almost independent of temperature in both deuterated cyclohexane (above the cloud point) and deuterated toluene. For dilute deuterated cyclohexane solutions the optically measured cloud point was found to be  $15 \pm 1$  °C. Two peaks were observed in the SANS data for the phase-separated (below the cloud point) deuterated cyclohexane solutions of the largest polymers (generation 3). The first peak (at smaller scattering vector) is attributed to the interference between molecules while the second peak arises from the single particle form factor which was also observed at temperatures above the cloud point. In deuterated cyclohexane the position of the form factor peak was constant at temperatures above 15 °C. In the phase-separated deuterated cyclohexane solutions the form factor peak shifted to higher  $q$ , indicating a fractional decrease in molecular diameter of about 15% upon phase separation. The spacing of the interference peak (at low  $q$ ) in the phase-separated solutions was consistent with the molecules aggregating in clusters with little interpenetration of the molecules. A power law function was used to model the real space density profile from which scattering curves were calculated and compared to the experimental data. This power law functional form for the density profile gave fits with smaller deviations from the experimental data when compared to either a hard or hollow sphere model.

## Introduction

Arborescent graft polymers are a general class of controlled architecture dendritic polymers such as dendrimers and hyperbranched polymers that have been developed by chemists in recent years.<sup>1–13</sup> Dendrimers are generally synthesized using stepwise, repetitive reaction sequences resulting in molecules with a highly regular shape, while hyperbranched polymers are synthesized in a single step by polycondensation and generally have an irregular shape. Arborescent graft polymers are branched macromolecules synthesized by successive cycles of functionalization and grafting reactions.<sup>7–13</sup> The molecules discussed here are synthesized from polystyrene grafted onto a polystyrene backbone, but the process is not restricted to one type of polymer and has also been demonstrated for a polystyrene core and a poly(ethylene oxide) shell.<sup>9</sup> Grafting linear polystyryl anions onto a partially chloromethylated linear polystyrene yields a generation 0 polymer as shown in Figure 1.<sup>7,8,12</sup> By repetition of the chloromethylation and anionic grafting reactions, higher generation polymers are synthesized. The grafting sites are believed to be distributed randomly throughout the molecule.<sup>7</sup> The structure of arborescent graft polymers is related to dendrimer molecules, but since the building blocks are polymer chains rather than monomers, arborescent graft polymers with very high molecular mass can be obtained within a few generations.<sup>7</sup> In

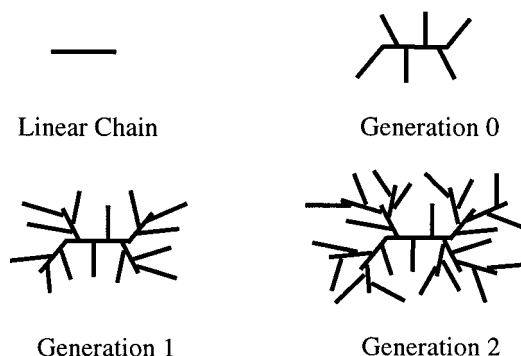


**Figure 1.** Schematic representation of the growth of arborescent graft polymers by successive cycles of chloromethylation and anionic grafting reactions.

addition, the grafting reaction in arborescent polymer molecules occurs randomly, as opposed to dendrimer molecules where the branching occurs at regular intervals throughout the structure. Since the branching in arborescent polymers is very dense, the distribution of graft sites becomes uniform throughout the molecule. The arborescent polymers should show spherical symmetry when the initial backbone molecular mass is comparable to the side chain molecular mass. An interesting characteristic of these systems is the possibility to synthesize well-defined macromolecules with a wide range of molecular mass and controlled shapes such as spheres, ellipsoids, and rods by varying the

branching density and/or the molecular weight of the initial backbone and/or the side chains.

There is little work in the literature on the intramolecular radial density profile of arborescent graft polymers, but there have been a number of both theoretical and computer simulation papers studying dendrimers.<sup>14–21</sup> For many of the proposed applications such as monomolecular micelles, flow modifiers, and drug delivery systems, the shape and internal structure of both arborescent graft polymers and dendrimers will play an important role. The first work on this topic was an analytical calculation by de Gennes and Hervet, who proposed a model with a minimum density at the center of the dendrimer molecule assuming long flexible spacers between the trifunctional monomer units.<sup>14</sup> Lescanec and Muthukumar have simulated the behavior of dendrimers by a kinetic growth method.<sup>15</sup> They found that dendrimer molecules with flexible branches exhibited a maximum density at the center of the molecule. Using a Monte Carlo simulation, Mansfield and Klushin<sup>16</sup> also found a maximum in the radial density profile at the center of the molecule with a density gradient to the outside edge of the molecule for smaller dendrimers, which is qualitatively similar to the result of Lescanec and Muthukumar. The larger generation dendrimers (generation 7) exhibited a weak local minimum at the center of the molecule.<sup>16</sup> Murat and Grest have investigated the effect of solvent quality on the density profile and size of dendrimers in solution using a molecular dynamics simulation.<sup>18</sup> The density profile of dendrimers under all solvent conditions revealed a high-density region near the core, a local minimum, and a constant density plateau followed by a transition zone in which the density decreased gradually.<sup>18</sup> They found that the average mean-squared radius of gyration increased as solvent quality increased. For example, the  $R_g$  of a generation 8 dendrimer increased by a factor of 1.5 in going from a poor solvent to a good solvent. Stechemesser and Eimer studied the influence of solvent quality on the size of dendrimers in solutions using holographic relaxation spectroscopy and found that the size of the molecules was not significantly different in various quality solvents for low generation dendrimers while solvent quality strongly influenced the size of high generation dendrimers.<sup>23</sup> Recent SANS, however, showed a less than 10% variation of the  $R_g$  of a generation 8 dendrimer in this range of solvents.<sup>24</sup> Stechemesser and Eimer suggested that for low generation dendrimers the configuration of the molecules was determined largely by the entropic part of the free energy, while the excluded-volume interaction between monomers gave only a minor contribution. According to the work of Naylor et al., the surface and internal volume accessible to the solvent increased with increasing generation number.<sup>20,21</sup> Thus, swelling is expected to increase with increasing solvent quality.<sup>23</sup> Another recent study by Boris and Rubinstein using a self-consistent mean-field calculation showed that the density is greatest at the core of the dendrimer and decays monotonically to the edge of the molecules.<sup>19</sup> Their result is in qualitative agreement with the density profile predicted by Lescanec and Muthukumar. Recently, Prosa et al. studied the internal structure of dendritic polymers using small-angle X-ray scattering (SAXS). By comparison of SAXS data with the scattering function calculated for various electron density distributions such as either a smooth or a rough sphere, they found that the density profile

for a generation 10 polyamidoamine (PAMAM) dendrimer does not exhibit any sizable minimum in density near the core.<sup>22</sup> More recent results by Prosa et al.<sup>25</sup> showed that large PAMAM dendrimers are spherical with a very uniform interior and a very narrow transition zone at the outside. Even dendrimers as small as a generation 4 dendrimer show spherelike characteristics.

The scaling relation for the size of branched polymers with molecular weight ( $R_g \sim M^{\nu}$ ) was first studied by Zimm and Stockmayer.<sup>26</sup> They found that for branched polymers the radius of gyration increased less rapidly with molecular mass than linear chains. They showed that, for a Cayley tree in which the chain lengths are randomly distributed,  $R_g \sim M^{0.5}$  for small values of the molecular mass and  $R_g \sim M^{0.25}$  for large values of the molecular mass. According to de Gennes and Hervet,<sup>14</sup> a perfect dendrimer can be grown up to a limiting generation number,  $m_l \cong 2.88(\ln P + 1.5)$  where  $P$  is the spacer length and the resultant scaling relation was given by  $R_g \sim M^{0.2}$ . Above this limit the growth of the dendrimers is imperfect, and compact structures with a constant density were expected ( $R_g \sim M^{0.33}$ ). Numerous computer simulations have been performed on dendrimers, and values of the scaling exponent reported have been in the range 0.2–0.4.<sup>15,17,18</sup> According to the computer simulations by Lescanec and Muthukumar, the scaling relation for a dendrimer with low molecular mass was  $R_g \sim M^{0.5}$  where  $R_g$  is the radius of gyration and  $M$  is the molecular mass.<sup>15</sup> For dendrimers with higher molecular mass (generations 5–7) the value of a scaling exponent was  $0.22 \pm 0.02$ , which is close to 0.25, the scaling exponent for a Cayley tree as calculated by Zimm and Stockmayer. Thus, their results indicated that as the dendrimers grow, the values of scaling exponent smoothly decrease with molecular mass, ultimately exhibiting Cayley treelike behavior. In the computer simulations by Mansfield and Klushin the value obtained was  $\nu = 0.4$  for dendrimers in a good solvent while Murat and Grest found that the  $R_g$  of dendrimers increases roughly as  $N^{1/3}$  under all solvent conditions ( $N$  being the number of monomer units).<sup>17,18</sup> Stechemesser and Eimer compared the scaling exponent of the dendrimers obtained from their experiments using holographic relaxation spectroscopy with the results from computer simulations.<sup>23</sup> The scaling exponent was in better agreement with the results given by Murat and Grest in comparison with the scaling behavior by Lescanec and Muthukumar. Star polymers in solution have been studied using intrinsic viscosity and SANS by Roovers et al.<sup>27–33</sup> In this work the range of functionality of the star polymers was from 8 to 128. The scaling exponent of a star polymer in a good solvent was measured using the Daoud–Cotton scaling model,  $R_g^2 \sim N^{2\nu} f^{-\nu}$  where  $N$  is the number of monomers per arm and  $f$  is the functionality. From these experiments  $\nu$  was found to be about 0.6.<sup>28,31,34</sup> Using viscosity measurements, Roovers et al. measured the ratio of hydrodynamic radius to the radius of gyration and found it to be close to  $(5/3)^{1/2}$ , the value for uniform density hard sphere, when  $f > 64$ .<sup>29,33</sup> Using SANS, Roovers et al. also compared the single particle form factor of star polymers with 128 arms with the scattering function for a hard sphere and argued that star polymer with 128 arms behaves as a hard sphere.<sup>31</sup>

Sheiko et al. studied the shape of arborescent graft polystyrenes in monomolecular films using scanning

atomic force microscopy (AFM) and found that the shape is dependent on the molecular mass and branching density.<sup>10</sup> A highly branched third generation arborescent polymer built from linear chains with a molecular mass of 5000 g/mol had a spherical shape discernible in the dry film, which was indicative of little interpenetration of the molecules. The density and diffusional properties of arborescent polymers were investigated using fluorescence quenching techniques by Frank et al.<sup>11</sup> They found that the segmental density of arborescent polymers in solution was significantly higher than for linear polystyrene. The diffusional properties of arborescent polymers indicated an increase in segmental density with increasing generation number.

The physical properties of branched polymers are significantly different from those of linear polymers. For example, the viscosity–molecular mass relation of dendrimers does not obey the Mark–Houwink–Sakurada equation. The intrinsic viscosity varies relatively slowly as a function of molecular mass compared to that of linear polymers, and a maximum is generally observed around generations 3–5.<sup>3,4</sup> On the other hand, the viscosity–molecular mass relation of hyperbranched polymers does obey the Mark–Houwink–Sakurada equation, but the viscosity is anomalously low compared to that of linear polymers.<sup>6</sup> The variation in the intrinsic viscosity as a function of molecular mass (generation number) for arborescent graft polymers is relatively small, similar to the trend for dendrimers.<sup>12</sup> Gauthier et al. found that the hydrodynamic radii calculated from the intrinsic viscosity measurements for arborescent polymers synthesized from side chains with a molecular mass of 5000 g/mol were essentially identical in a  $\Theta$  solvent (cyclohexane) and a good solvent (toluene). But for arborescent polymers with a higher molecular mass side chains (30 000 g/mol), significant expansion was observed in toluene, and the increase was largest for the higher generation molecules.

In this paper small-angle neutron scattering (SANS) was used to determine the size and the density profile of arborescent graft polymers in solution as a function of temperature and molecular mass (generation number). Deuterated cyclohexane and deuterated toluene were used as solvents. Deuterated cyclohexane is a  $\Theta$  solvent for the linear polystyrene with a  $\Theta$  temperature of 40 °C.<sup>35</sup> Deuterated toluene is a good solvent for the linear polystyrene. In previous light scattering studies by Gauthier et al., the second virial coefficient,  $A_2$ , for arborescent graft polymers in cyclohexane was found to be close to zero with negligible variation as a function of temperature, indicating that cyclohexane was effectively a  $\Theta$  solvent at all temperatures studied.<sup>13</sup>

## Experimental Section

The synthesis of the arborescent graft polymers used in this study has been discussed elsewhere.<sup>12</sup> The molecular mass of the individual branches grafted for each generation was determined by gel permeation chromatography. The mass average molecular mass,  $M_w$ , of the arborescent polymers was determined as part of the SANS experiments described in this paper. The characteristics of the arborescent graft polymers are given in Table 1. These polymers have a linear core and side chains with a molecular mass of 5000 g/mol. The total number of branches in a generation  $G$  polymer was calculated using eq 1:

$$f_w(\text{tot}) = f_w(G-1) + \frac{M_w(G) - M_w(G-1)}{M_w(\text{branch})} \quad (1)$$

**Table 1. Characteristics of Arborescent Graft Polymers with 5000 g mol<sup>-1</sup> Branches**

generation	branches		graft polymer		
	$M_w/10^3$ g mol <sup>-1</sup>	$M_w/M_n$	$M_w$ / g mol <sup>-1</sup>	$f_w(\text{tot})$	branching density
0	4.3	1.03	$5.7 \times 10^4$	12	0.25
1	4.6	1.03	$5.7 \times 10^5$	120	0.20
2	4.2	1.04	$3.2 \times 10^6$	720	0.11
3	4.4	1.05	$2.4 \times 10^7$	5200	0.15

where  $M_w(G)$ ,  $M_w(G-1)$ , and  $M_w(\text{branch})$  are the molar masses of generation  $G$ , the previous generation, and the grafted side chains, respectively. If the molecular mass of the branches for each generation is the same, eq 1 can be reduced to a simpler form:

$$f_w(\text{tot}) = \frac{M_w(G) - M_w(\text{linear core})}{M_w(\text{branch})} \quad (2)$$

The branching density of the core portion of a generation  $G$  polymer is given by eq 3:

$$\text{branching density} = \frac{\text{no. of branches added per molecule in a grafting reaction}}{\text{total no. of repeat units of previous generation}} \quad (3)$$

Deuterated cyclohexane and deuterated toluene used as solvents for the arborescent polymers were purchased from Cambridge Isotope Laboratories, Inc.<sup>36</sup> The concentration range of the solutions studied was  $\phi = 0.005$ – $0.015$  mass fraction. Before performing small-angle neutron scattering experiments, the optical cloud point was measured for 0.0025 mass fraction solutions. Since arborescent polymer solutions in deuterated cyclohexane exhibit an upper critical solution temperature (UCST), phase separation is expected on cooling below the  $\Theta$  temperature (40 °C). The cloud point for generation 3 was found to be about 15 °C by cooling the sample in an oil bath and observing the temperature when the solution became cloudy. Phase separation could not be observed by this method for solutions of generation 0, 1, and 2 polymers down to 10 °C, which is close to the freezing point of deuterated cyclohexane. The temperature was varied from 60 to 10 °C in the SANS experiments.

Small-angle neutron scattering experiments were carried out at the Center for Neutron Research at the National Institute of Standards and Technology on the 30 m NIST-NG3 instrument.<sup>37,38</sup> The raw data were corrected for scattering from the empty cell, incoherent scattering, detector dark current, detector sensitivity, sample transmission, and thickness. Following these corrections the data were placed on an absolute scale using a calibrated secondary standard and circularly averaged to produce  $I(q)$  versus  $q$  plots where  $I(q)$  is the scattered intensity and  $q$  is the scattering vector. The  $q$  range was varied from 0.0046 to 0.0520 Å<sup>-1</sup> with a neutron wavelength of  $\lambda = 6$  Å and a wavelength spread of  $\Delta\lambda/\lambda = 0.15$ .

The uncertainties are calculated as the estimated standard deviation of the mean, and the total combined uncertainty is not given as comparisons are made with data obtained under the same conditions. In cases where the limits are smaller than the plotted symbols, the limits are left out for clarity. Fits of the scattering data are made by a least squares, giving an average and a standard deviation to the fit. All temperatures reported are within  $\pm 1$  °C as determined by previous experience.

## Results and Discussion

A typical set of SANS data for all arborescent polymer generations ( $T = 30$  °C,  $\phi = 0.005$  mass fraction in deuterated cyclohexane) is shown in Figure 2. The radii of gyration were measured using Guinier plots at small

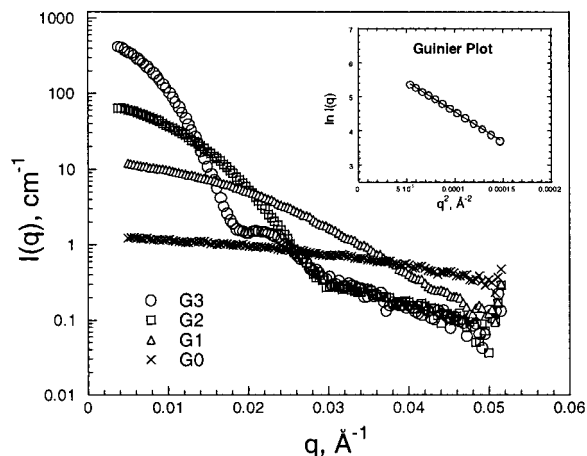


**Figure 2.** SANS curves for all generations at 30 °C. Inset shows a typical Guinier plot used to obtain  $R_g$ .

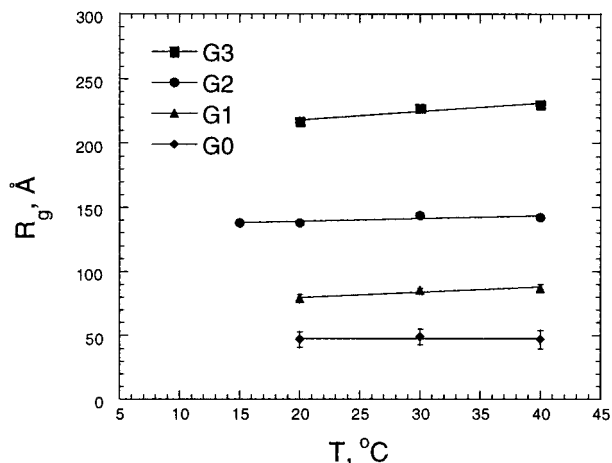


**Figure 3.**  $R_g$  for arborescent graft polymers in *d*-cyclohexane versus temperature.

$q$ . For dilute noninteracting particles the scattering intensity is expected to obey Guinier's law:

$$I(q) = I(0) \exp\left(-\frac{R_g^2 q^2}{3}\right) \quad (4)$$

where  $R_g$  is the radius of gyration of the object.<sup>39,40</sup> A typical Guinier plot of  $\ln I(q)$  versus  $q^2$  for a generation 3 polymer is displayed as an inset in Figure 2. The variations in  $R_g$  obtained from Guinier plots as a function of temperature are shown for the different generation polymers in deuterated cyclohexane in Figure 3 and in deuterated toluene in Figure 4. The error bars represent standard deviation calculated from the linear least-squares fit from the Guinier plots. As can be seen from Figures 3 and 4, the size of arborescent polymers in both solvents is essentially independent of temperature in the range investigated. For generations 0 and 1 the size of the molecules is equivalent in the two solvents, while for generations 2 and 3 the molecules are significantly expanded (particularly for generation 3) in deuterated toluene. This result differs from the hydrodynamic radius values obtained from intrinsic viscosity by Gauthier et al., who found that the hydrodynamic radius values were essentially identical in toluene and cyclohexane for polymers with 5000 g/mol side chains.<sup>12</sup> They did observe significant expansion in toluene for arborescent polymers with a 30 000 g/mol branches, however. It is reasonable to assume that for

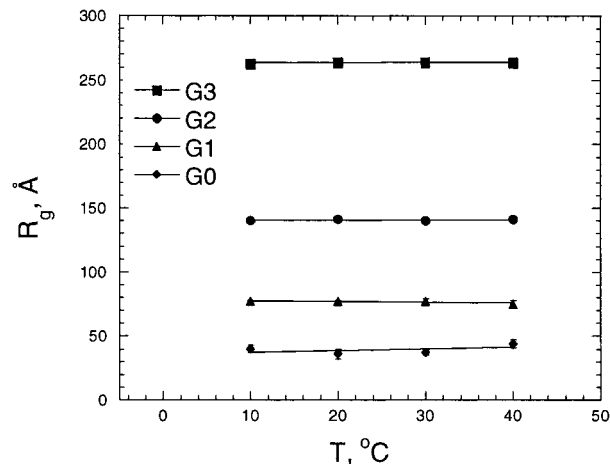


**Figure 4.**  $R_g$  for arborescent graft polymers in *d*-toluene versus temperature.

low generation arborescent polymers the entropic part of the free energy dominates the configuration of the molecules, while for higher generation polymers the interaction energy between segments is dominant. For generation 3 the  $R_g$  ratio of the polymer in deuterated toluene to that in deuterated cyclohexane is about 1.2.

By taking the limit as  $q \rightarrow 0$  for the Zimm equation, one obtains<sup>41–45</sup>

$$\frac{k_n \phi_a}{I(0)} = \frac{1}{\langle N_a \rangle_w v_a} + 2A_2 \phi_a \quad (5)$$

where  $I(q)$  is the measured scattered intensity,  $\phi_a$  is the mass fraction of the dilute polymer,  $\langle N_a \rangle_w$  is the mass average degree of polymerization of the polymer,  $v_a$  is its specific volume,  $A_2$  is the second virial coefficient and  $k_n$  is the contrast factor for neutrons. The mass average molecular mass and the second virial coefficient can be thus determined from a plot of  $\phi_a/I(0)$  versus  $\phi_a$  using the  $\phi/I(0)$  values obtained from Guinier plots at  $q = 0$ . Values for  $\langle N_a \rangle_w$  were obtained from the intercept of the line with the  $y$ -axis using eq 5, and the second virial coefficients were calculated from the slope of the line. Previous SANS experiments have demonstrated that measurements of this nature have a standard uncertainty of  $\pm 5\%$ . The second virial coefficients determined in this manner are plotted as a function of inverse temperature in Figure 5. Since generation 0 has a low branching functionality, it is reasonable that  $A_2$  decreases as a function of temperature from 60 to 20 °C as deuterated cyclohexane becomes a  $\Theta$  solvent for polystyrene. For generation 1 and above,  $A_2$  is essentially zero for all temperatures between 20 and 60 °C. The second virial coefficient in deuterated toluene was not studied since only one concentration (mass fraction,  $\phi = 1\%$ ) was prepared for the SANS experiments. Gauthier et al. have studied the temperature dependence of the second virial coefficient for arborescent polystyrenes in solution using light scattering and found that  $A_2$  is more strongly influenced by the branching functionality than by the overall molecular mass of the polymers.<sup>13</sup> According to their study of arborescent polymers in cyclohexane,  $A_2$  was dependent on temperature only for the generation 0 polymer with 5000 g/mol side chains while  $A_2$  was close to zero with negligible variation for the generation 1 polymer, which indicates the polymer is essentially at  $\Theta$  conditions (based on  $A_2$ ) for all measured temperatures in cyclo-

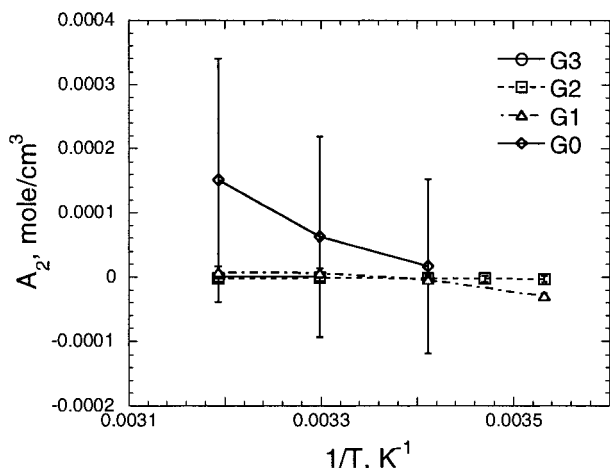


**Figure 5.**  $A_2$  versus inverse temperature for all generations of arborescent graft polymers in *d*-cyclohexane.

hexane. A generation 0 polymer with 30 000 g/mol side chains which had a comparable molecular mass but lower branching functionality than the generation 1 polymer with 5000 g/mol side chains was found to have a significant temperature dependence of  $A_2$ . This indicated that the branching functionality has more influence on the temperature dependence of  $A_2$  than the side chain molecular mass. The temperature dependence of  $A_2$  for higher generation polymers was not studied by Gauthier et al.

A log–log plot of  $M_w$  versus  $R_g$  for the arborescent polymers in deuterated cyclohexane is shown in Figure 6a. A scaling relation given by  $R_g = kM^\nu$  exists between  $R_g$  and the molecular mass,  $M_w$ , where  $\nu$  is the scaling factor and  $k$  is a constant. One can expect two limiting cases in Figure 6a. A Gaussian linear polymer chain should have an exponent of  $\nu = 1/2$  under  $\Theta$  conditions. For an object with constant density (such as a hard sphere) a scaling exponent of  $\nu = 1/3$  is expected. Arborescent polymers should probably exhibit a crossover between these two behaviors, with the low generation materials behaving (relatively) as a linear Gaussian polymer but becoming more dense as the branching functionality increases with increasing generations. The ultimate limit would be attained if the molecules reach constant density ( $\nu = 1/3$ ), although this exponent probably would not be expected to be observed for arborescent polymers dispersed in solution. Two lines are shown in Figure 6a, one calculated for linear Gaussian polystyrene chains under  $\Theta$  conditions ( $\nu = 1/2$ ) and one for spheres with the bulk density of polystyrene, assuming the chains are completely collapsed. For the generation 0 polymer the observed  $R_g$  in deuterated cyclohexane is somewhat smaller than expected for a linear chain. For the largest polymer (generation 3) the molecular mass is much higher than expected for a linear Gaussian coil of equivalent  $R_g$ , resulting in a significantly higher polymer segment density within the effective sphere defined by the radius of gyration. Although the data in Figure 6a appear to fall on a straight line and yield a exponent of  $\nu = 0.25 \pm 0.01$ , it should be pointed out that the chain architecture is changing dramatically with increasing generation. The standard uncertainties are calculated from the goodness of the fit and are not plotted in Figure 6 for clarity. The exponent of  $\nu = 0.25$  indicates that the average polymer segment density inside the coil is increasing, which is a naturally self-limiting process as

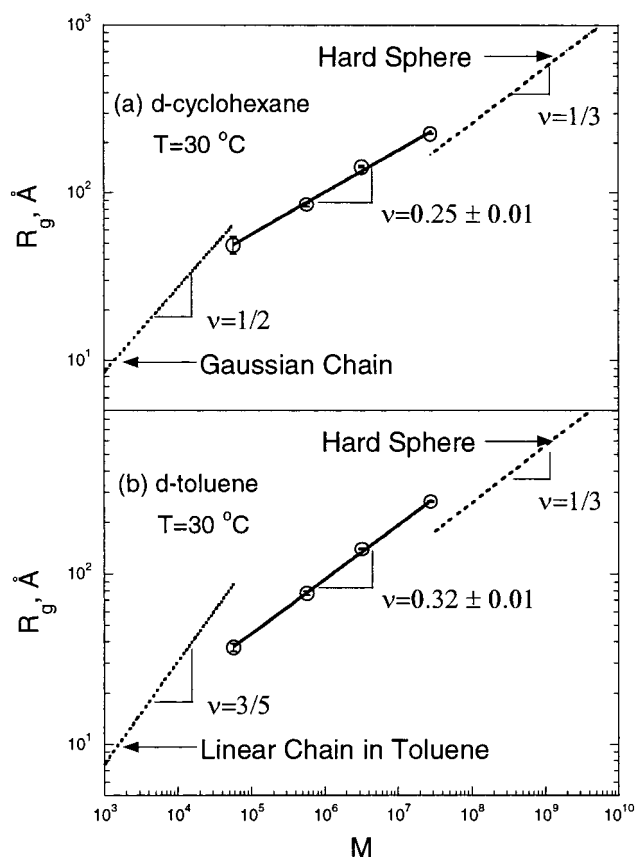


**Figure 6.** (a)  $R_g$  versus molecular mass for arborescent graft polymer in *d*-cyclohexane. (b)  $R_g$  versus molecular mass for arborescent graft polymer in *d*-toluene.

bulk density is approached. The line through the data in Figure 6a should probably be considered crossover behavior with the exponent of  $\nu = 0.25$  depending on the details of the arborescent polymer architecture (branch length, branching density, etc.). A log–log plot of  $M_w$  versus  $R_g$  for the arborescent polymers in deuterated toluene is shown in Figure 6b. The line for linear polystyrene in toluene was obtained by a linear least-squares fit to the data for polystyrene in toluene obtained using small-angle X-ray scattering (SAXS) and light scattering by Abe et al.<sup>46–48</sup> For arborescent polymers in deuterated toluene a crossover behavior between a linear chain ( $\nu = 3/5$ ) and dense object ( $\nu = 1/3$ ) is expected. For the low generation polymers the observed  $R_g$  in deuterated toluene is expected to approach that of a linear chain in a good solvent, while the behavior of the high generation polymers approaches that of an object of constant density. The scaling exponent of  $0.32 \pm 0.01$  indicates that the polymer segment density of arborescent polymers dissolved in deuterated toluene relatively increases slowly as a function of generation in comparison with the same polymer dissolved in deuterated cyclohexane.

The SANS data for generation 3 polymers clearly show a Guinier region and a second interference peak at higher  $q$ . This second peak is characteristic of single particles with a relatively uniform size distribution. Attempts to fit the data for generation 3 in both deuterated cyclohexane and deuterated toluene using a simple model such as a hard sphere were not successful. Scattering curves calculated for various core/shell models (with a lower density in the interior of the molecule as suggested by de Gennes and Hervet) actu-

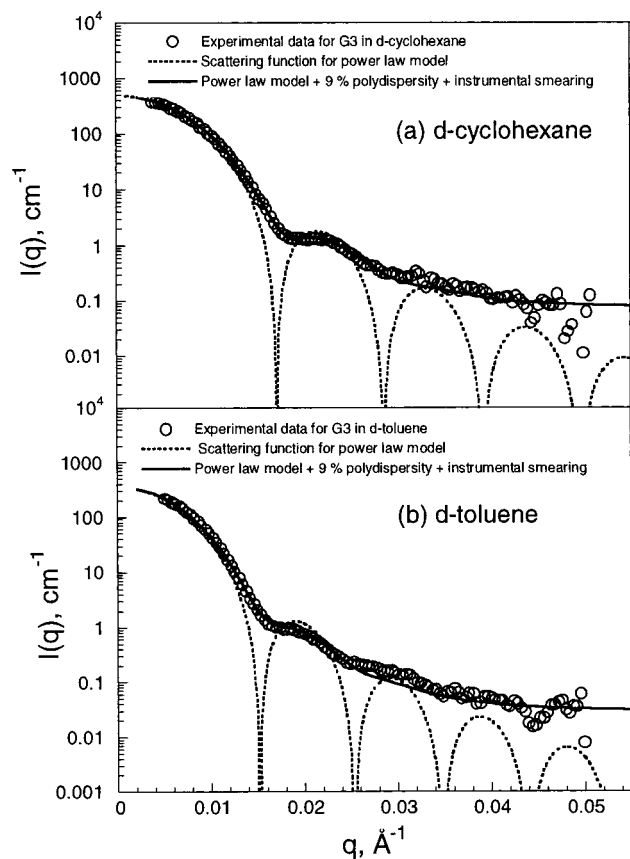


**Figure 7.** (a) Scattering calculated using the power law model compared experimentally measured scattering for generation 3 polymer in *d*-cyclohexane. (b) Scattering calculated using the power law model compared with experimentally measured scattering for generation 3 polymer in *d*-toluene.

ally fit the data worse than that for a hard sphere model. As an alternative model, a power law density function was used to fit the data as suggested by Neese et al. for polystyrene microgels.<sup>49</sup> The function used is given by

$$\rho(r) = 1 - \left(\frac{r}{R_{\max}}\right)^{\alpha} \quad (6)$$

where  $R_{\max}$  corresponds to the hydrodynamic radius. When  $\alpha$  goes to infinity, this model is equivalent to a hard sphere model. The fit to the data was optimized by varying the value of  $\alpha$  and calculating the scattering using eq 7.<sup>50,51</sup>

$$I(q) \propto \left[ \int dr \rho(r) \frac{\sin(qr)}{qr} r^2 \right]^2 \quad (7)$$

The scattering calculated using the power law model with  $\alpha > 4$  was found to lie significantly above the experimental scattering data while the calculated scattering with  $\alpha < 4$  was found to lie below the data. The power law model with  $\alpha = 4$  gave a fit with the smallest deviation from the experimental data and is shown for the generation 3 polymer in deuterated cyclohexane and deuterated toluene in Figure 7a,b. The fit of the data in Figure 7a,b includes a 9% polydispersity in size for the polymer and the effect of instrumental smearing (see Appendix) with  $I(0)$ ,  $R_{\max}$ , and a baseline as floating parameters. The values of  $R_{\max} = 310 \pm 6 \text{ \AA}$  and  $R_{\max} = 350 \pm 8 \text{ \AA}$  were obtained from the fit of the scattering data in Figure 7a,b for the generation 3 polymer in

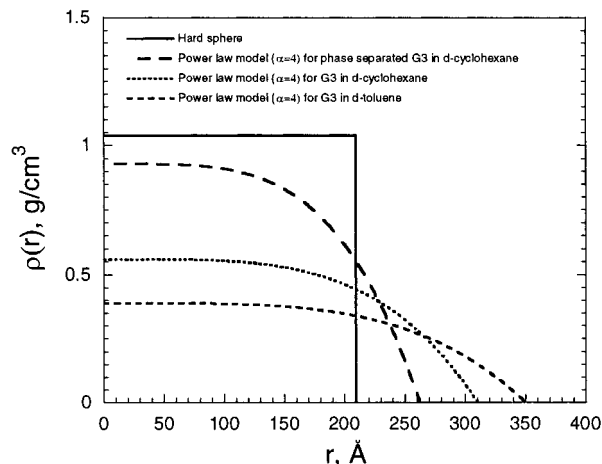


**Figure 8.** Radial density profile for the power law model and hard sphere model (for comparison).

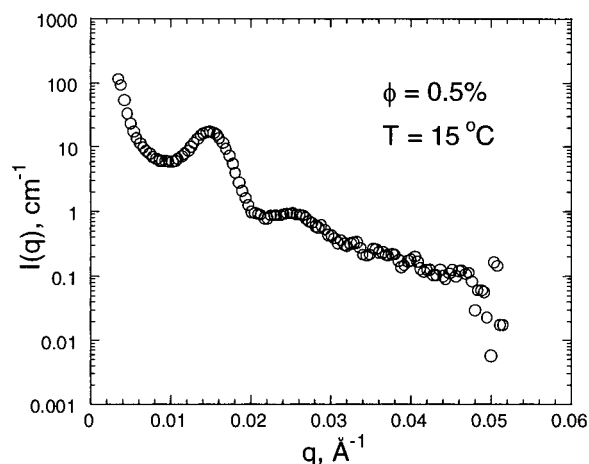


**Figure 9.**  $I(q)$  versus  $q$  for phase separated generation 3 polymer in *d*-cyclohexane ( $T = 15 \text{ }^\circ\text{C}$ ).

deuterated cyclohexane and deuterated toluene, respectively. The errors were calculated from the errors in  $q$  based on the SANS instrument configuration. A comparison of the radial density profile calculated with  $\alpha = 4$  with that of a hard sphere in bulk density is shown in Figure 8. Each density function in Figure 8 was normalized to have equal molecular mass of the generation 3 polymer. Thus, integration of the density profiles with respect to volume shown in Figure 8 gives the same value for the mass of a molecule.

For the arborescent graft polymers in deuterated toluene the samples were not phase-separated at  $10 \text{ }^\circ\text{C}$  (which is the lowest temperature studied in this work), and the scattering was almost unchanged between  $40$  and  $10 \text{ }^\circ\text{C}$ . Phase separation for the generation 3 polymer in deuterated cyclohexane was observed optically at  $15 \text{ }^\circ\text{C}$ . The dense polymer rich phase was allowed to settle to the bottom of the sample cell, and the scattering measured from this phase is shown in Figure 9. Two peaks were found in the  $I(q)$  versus  $q$  data. The first peak is due to the interference between molecules, while the second peak arises from the single particle form factor. From the position of the first peak the center-to-center distance between nearest-neighbor molecules was estimated using the relation  $d = (1.23 \times 2\pi)/q$ , for a structure controlled by two body noncrystalline correlations.<sup>39,40</sup> This distance was found to be  $518 \pm 14 \text{ \AA}$ . From the position of the second peak, the diameter of a single molecule was estimated using the

**Table 2.**  $R_{\max}$  and  $R_g$  of Generation 3 as a Function of Temperature in *d*-Cyclohexane Obtained by Fitting the Peak Using a Single Particle Scattering Function Which Is Derived from Density Profile,  $\rho = 1 - (r/R_{\max})^4$

temperature (°C)	$R_{\max}$ (Å)	$R_g$ (Å)
40	310 ± 6	212 ± 5
30	317 ± 6	217 ± 5
20	306 ± 5	209 ± 4
15	262 ± 5	179 ± 4

single particle scattering function derived from the density profile (eq 6). The data in the range of  $q = 0.018\text{--}0.05 \text{ \AA}^{-1}$  were fit to the scattering function calculated using the power law model ( $\alpha = 4$ ).  $R_{\max}$  was found to be  $262 \pm 5 \text{ \AA}$ , and the calculated density profile for phase-separated generation 3 polymer in deuterated cyclohexane is shown in Figure 8. The errors for the value of  $R_{\max}$  were calculated from the errors in  $q$  based on the SANS instrument configuration. The diameter of a single molecule is  $d_{\max} = 2R_{\max} = 524 \pm 10 \text{ \AA}$ , which is very close to the distance between nearest neighbors, indicating that the molecules are just in contact with each other with very little interpenetration. The position of the second peak in the  $I(q)$  versus  $q$  plots from the single molecule scattering form factor was used to monitor the radius of the molecule,  $R_{\max}$  as a function of temperature. Using the power law density function given by eq 6, the radius of gyration was calculated from eq 8 and was found to be  $R_g = (7/15)^{1/2} R_{\max}$  (for  $\alpha = 4$ ) as compared to  $R_g = (3/5)^{1/2} R_{\max}$  for a hard sphere.

$$R_g^2 = \frac{\int dr \rho(r) r^4}{\int dr \rho(r) r^2} \quad (8)$$

Table 2 shows  $R_{\max}$  and  $R_g$  calculated for the polymers in *d*-cyclohexane as a function of temperature.

For comparison, the  $R_g$  of a sphere was calculated assuming that the generation 3 molecules were collapsed to bulk density. The  $R_g$  obtained was approximately  $162 \text{ \AA}$ , which is close to the  $R_g$  of the generation 3 polymer in deuterated cyclohexane at  $15 \text{ }^\circ\text{C}$  in Table 2. This indicates that the generation 3 molecules should be essentially noninterpenetrating after phase separation, and deuterated cyclohexane is largely excluded from the arborescent polymer molecules.

The first observation of the collapse transition in a linear polystyrene chain in cyclohexane has been reported by Swislow et al.<sup>52</sup> They found that the hydrodynamic radius of a polystyrene chain in cyclohexane decreases sharply by a factor of 60% as the temperature is lowered below the  $\Theta$  temperature. Chu et al. have investigated the polystyrene/cyclohexane system extensively using light scattering.<sup>53–55</sup> According to their study, the collapsed state observed on the basis of  $R_g$  values corresponds to a relative contraction of about 15%. Bauer and Ullman studied the contraction of polystyrene in cyclohexane below  $\Theta$  temperature as a function of molecular mass.<sup>56</sup> For low molecular mass polystyrene they observed a gradual decrease in the expansion coefficient with decreasing temperature and sharp decrease for high molecular mass polystyrene. To follow the change in size of the generation 3 polymer in deuterated cyclohexane, the  $R_g$  was measured at  $2 \text{ }^\circ\text{C}$  intervals between  $30$  and  $7 \text{ }^\circ\text{C}$ , and the data obtained are shown in Figure 10. A collapse of the generation 3 molecules by about 15% was observed over the temperature range of  $14\text{--}9 \text{ }^\circ\text{C}$ .

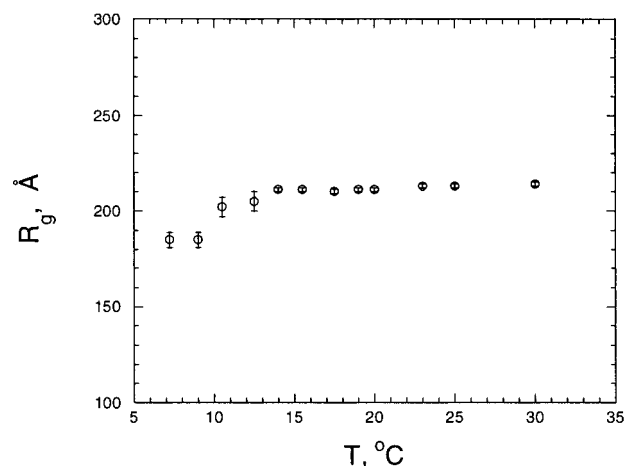


**Figure 10.**  $R_g$  for generation 3 polymer in *d*-cyclohexane versus temperature showing the collapse of the molecule upon phase separation.

## Conclusions

The radius of gyration of arborescent graft polymers in solution was measured by SANS and found to increase with increasing generation (molecular mass). In going from deuterated toluene (a good solvent) to deuterated cyclohexane (a  $\Theta$  solvent), the  $R_g$  of the largest molecules (generations 2 and 3) was observed to decrease. No significant change in size was observed for the smaller generations. The scaling exponent for  $R_g \sim M^\nu$  was found to be  $\nu = 0.25 \pm 0.01$  in deuterated cyclohexane and  $\nu = 0.32 \pm 0.01$  in deuterated toluene. This value of  $\nu$  is less than that for both a hard sphere and a Gaussian linear polymer chain and indicates that the arborescent polymer segment density is increasing as a function of generation. This exponent probably represents crossover behavior and is presumably dependent on the specific architecture of the arborescent polymers. A power law model for the radial density function was used to fit the data, and reasonable agreement with the experimental scattering was obtained. The size of arborescent polymer molecules in deuterated toluene was essentially independent of temperature down to  $10 \text{ }^\circ\text{C}$ . The radius of gyration of arborescent polymers in deuterated cyclohexane was found to be almost independent of temperature down to the phase separation temperature ( $15 \text{ }^\circ\text{C}$ ) where precipitation was observed, with a concomitant abrupt fractional decrease in  $R_g$  by about 15%. In the two-phase solution the polymer molecules were observed to aggregate in the polymer-rich phase, and the scattering from this phase indicated that the molecules are essentially noninterpenetrating and close packed with liquid type ordering.

**Acknowledgment.** This work has benefited from the use of the 30 m NIST-NG3 instrument at the Center for Neutron Research at the National Institute of Standards and Technology. It is based upon activities supported by the National Science Foundation under Agreement DMR-9423101. We acknowledge the support of the National Institute of Standards and Technology, U.S. Department of Commerce, in providing the neutron research facilities used in this experiment. The authors thank Dr. J. Barker and Dr. S. Klein at NIST for help with the SANS experiments and data analysis. A. Topp gratefully acknowledges the financial support by the Deutsche Forschungsgemeinschaft. M. Gauthier acknowledges the financial support of the Natural Sciences and

Engineering Research Council of Canada. This material is based upon work supported in part by the U.S. Army Research Office under Contract 35109-CH.

## Appendix

The instrumental smearing due to scattering such as the geometry and wavelength spread alters the measured intensity from the true scattering intensity.<sup>57–59</sup> The resolution function can be approximated by Gaussian function<sup>57,58</sup>

$$R(q, \bar{q}) = (2\pi V_q)^{-1/2} \exp[(q - \bar{q})^2/2 V_q] \quad (9)$$

where the variance,  $V_q$ , and the mean scattering vector,  $\bar{q}$ , are a function of  $q_0$ , which corresponds to the instrument configuration. The scattering vector,  $q_0$ , is defined as

$$q_0 = 4\pi \sin(\theta_0/2)/\lambda_0 \quad (10)$$

where  $\lambda_0$  is the wavelength of the incident neutrons. The scattering angle,  $\theta_0$ , is given by

$$\theta_0 = \tan^{-1}(r_0/L) \quad (11)$$

where  $r_0$  is the distance between the center of the beam and the center of the detector element in the detector plane and  $L$  is the sample-to-detector distance.  $V_q$  is given by

$$V_q \cong q_0^2 [(V_r/r_0^2) + (V_\lambda/\lambda_0^2)] \quad (12)$$

$V_r$  is related to the distance variance from the beam divergence, the distance variance from the detector resolution, and the distance variance from gravity.  $V_\lambda$  is related to the wavelength spread,  $\Delta\lambda_0/\lambda_0$ . By considering the distribution of scattering vectors with length,  $q$ , which contribute to  $q_0$ , the smeared intensity is calculated as

$$I_s(q_0) = \int_0^\infty dq R(q, q_0) I(q) \quad (13)$$

where  $I(q)$  is the absolute scattering intensity.

## References and Notes

- Tomalia, D. A.; Baker, H.; Dewald, J.; Hall, M.; Kalos, G.; Martin, S.; Roeck, J.; Ryder, J.; Smith, P. *Polym. J.* **1985**, *17*, 117.
- Tomalia, D. A.; Naylor, A. M.; Goddard, W. A. *Angew. Chem., Int. Ed. Engl.* **1990**, *29*, 138.
- Tomalia, D. A.; Hedstrand, D. M.; Wilson, L. R. *Encyclopedia of Polymer Science and Engineering*, 2nd ed., John Wiley & Sons: New York, 1990; Vol. 46.
- Mourey, T. H.; Turner, S. R.; Rubinstein, M.; Fréchet, J. M. J.; Hawker, C. J.; Wooley, K. L. *Macromolecules* **1992**, *25*, 2401.
- Kim, Y. H.; Webster, O. W. *J. Am. Chem. Soc.* **1990**, *112*, 4592.
- Turner, S. R.; Voit, B. I.; Mourey, T. H. *Macromolecules* **1993**, *26*, 4617.
- Gauthier, M.; Möller, M. *Macromolecules* **1991**, *24*, 4548.
- Gauthier, M.; Möller, M.; Burchard, W. *Macromol. Symp.* **1994**, *77*, 43.
- Gauthier, M.; Tichagwa, L.; Downey, J. S.; Gao, S. *Macromolecules* **1996**, *29*, 519.
- Sheiko, S. S.; Gauthier, M.; Möller, M. *Macromolecules* **1997**, *30*, 2343.
- Frank, R. S.; Merkle, G.; Gauthier, M. *Macromolecules* **1997**, *30*, 5397.
- Gauthier, M.; Li, W.; Tichagwa, L. *Polymer* **1997**, *38*, 6363.
- Gauthier, M.; Chung, J.; Choi, L.; Nguyen, T. T. *J. Phys. Chem. B* **1998**, *102*, 3138.
- de Gennes, P. G.; Hervet, H. *J. Physiol. Lett.* **1983**, *44*, L351.
- Lescanec, R. L.; Muthukumar, K. *Macromolecules* **1990**, *23*, 2280.
- Mansfield, M. L.; Klushin, L. I. *Macromolecules* **1993**, *26*, 4262.
- Mansfield, M. L. *Polymer* **1994**, *35*, 1827.
- Murat, M.; Grest, G. S. *Macromolecules* **1996**, *29*, 1278.
- Boris, D.; Rubinstein, M. *Macromolecules* **1996**, *29*, 7251.
- Naylor, A. M.; Goddard, W. A. *Polym. Prepr.* **1988**, *29*, 215.
- Naylor, A. M.; Goddard, W. A.; Keifer, G.; Tomalia, D. A. *J. Am. Chem. Soc.* **1989**, *111*, 2339.
- Prosa, T. J.; Bauer, B. J.; Amis, E. J.; Tomalia, D. A.; Scherrenberg, R. J. *Polym. Sci.* **1997**, *35*, 2913.
- Stechemesser, S.; Eimer, W. *Macromolecules* **1997**, *30*, 2204.
- Topp, A.; Bauer, B. J.; Tomalia, D. A.; Amis, E. J. Accepted in *Macromolecules*.
- Prosa, T. J.; Bauer, B. J.; Amis, E. J. To be submitted.
- Zimm, B. H.; Stockmayer, W. H. *J. Chem. Phys.* **1949**, *17*, 1301.
- Zhou, L. L.; Hadjichristidis, N.; Toporowski, P. M.; Roovers, J. *Rubber Chem. Technol.* **1992**, *65*, 303.
- Richter, D.; Jucknischke, O.; Willner, L.; Fetters, L. J.; Lin, M.; Huang, J. S.; Roovers, J.; Toporowski, C.; Zhou, L. L. *J. Phys. (Paris)* **1993**, *3*, 3.
- Roovers, J.; Zhou, L. L.; Toporowski, P. M.; Zwan, M.; Iatrou, H.; Hadjichristidis, N. *Macromolecules* **1993**, *26*, 4324.
- Roovers, J. *Macromolecules* **1994**, *27*, 5359.
- Willner, L.; Jucknischke, O.; Richter, D.; Roovers, J.; Zhou, L. L.; Toporowski, P. M.; Fetters, L. J.; Huang, J. S.; Lin, M. Y.; Hadjichristidis, N. *Macromolecules* **1994**, *27*, 3821.
- Roovers, J.; Toporowski, P. M.; Douglas, J. *Macromolecules* **1995**, *28*, 7064.
- Roovers, J. *Macromol. Symp.* **1997**, *121*, 89.
- Daoud, M.; Cotton, J. P. *J. Phys. (Paris)* **1982**, *43*, 531.
- Strazielle, C.; Benoit, H. *Macromolecules* **1975**, *8*, 203.
- Certain commercial materials and equipment are identified in this paper in order to specify adequately the experimental procedure. In no case does such identification imply recommendation by the National Institute of Standards and Technology nor does it imply that the material or equipment identified is necessarily the best available for this purpose.
- NG3 and NG7 30-meter SANS Instruments Data Acquisition Manual*, National Institute of Standards and Technology Cold Neutron Research Facility, 1996.
- Glinka, C. J.; Barker, J. G.; Hammouda, B.; Krueger, S.; J. Moyer, J. J.; Orts, W. J. *J. Appl. Crystallogr.* **1998**, *31*, 430.
- Guinier, A.; Fournet, G. *Small Angle Scattering of X-Rays*; Wiley: New York, 1955.
- Guinier, A. *X-Ray Diffraction*; W. H. Freeman and Company: San Francisco, 1963.
- Sakurai, S.; Hasegawa, H.; Hashimoto, T.; Han, C. C. *Polym. Commun.* **1990**, *31*, 99.
- Maconnachie, A.; Kambour, R. P.; White, D. M.; Rostami, S.; Walsh, D. J. *Macromolecules* **1984**, *17*, 2645.
- Zimm, B. H. *J. Chem. Phys.* **1948**, *16*, 1093.
- Zimm, B. H. *J. Chem. Phys.* **1948**, *16*, 1099.
- Briber, R. M.; Bauer, B. J.; Hammouda, B. *J. Chem. Phys.* **1994**, *101*, 2592.
- Abe, F.; Einaga, Y.; Yoshizaki, T.; Yamakawa, H. *Macromolecules* **1993**, *26*, 1884.
- Abe, F.; Einaga, Y.; Yoshizaki, T.; Yamakawa, H. *Macromolecules* **1993**, *26*, 1891.
- Abe, F.; Einaga, Y.; Yoshizaki, T.; Yamakawa, H. *Macromolecules* **1993**, *26*, 1898.
- Neese, M. Private discussions.
- Higgins, J. S.; Benoit, H. C. *Polymers and Neutron Scattering*; Oxford Science Publications: Oxford, 1994.
- Feigin, L. A.; Svergun, D. I. *Structure Analysis by Small Angle X-Ray and Neutron Scattering*; Plenum Press: New York, 1987.
- Swislow, G.; Sun, S.; Nishio, I.; Tanaka, T. *Phys. Rev. Lett.* **1980**, *44*, 796.
- Chu, B.; Wang, J. *Macromolecules* **1989**, *22*, 380.
- Park, I. H.; Wang, Q. W.; Chu, B. *Macromolecules* **1987**, *20*, 1965.
- Chu, B.; Park, I. H.; Wang, Q. W.; Wu, C. *Macromolecules* **1987**, *20*, 2833.
- Bauer, D. R.; Ullman, R. *Macromolecules* **1980**, *13*, 392.
- Barker, J. G.; Pedersen, J. S. *J. Appl. Crystallogr.* **1995**, *28*, 105.
- Mildner, D. F. R.; Carpenter, J. M. *J. Appl. Crystallogr.* **1984**, *17*, 249.
- Glatter, O. *Modern Methods of Data Analysis in Small Angle Scattering and Light Scattering*; Kluwer Academic Publishers: Dordrecht, 1995.